

# Numerical Methods for Simulating Brake Squeal Noise

S. Oberst\*, J.C.S. Lai

Acoustics & Vibration Unit, School of Engineering and Information Technology,  
The University of New South Wales, Australian Defence Force Academy, Canberra, ACT 2600, Australia

PACS: 4001ss

## ABSTRACT

Due to significantly reduced interior noise as a result of reduction of noise from internal combustion engine and tyre-road contact noise and the use of lightweight composite materials for the car body, disc brake squeal has become increasingly a concern to automotive industry because of the high costs in warranty related claims. While it is now almost standard practice to use the complex eigenvalue method in commercial finite element codes to predict unstable vibration modes, not all predicted unstable vibration modes will squeal and vice versa. There are very few attempts to calculate the acoustic radiation from predicted unstable vibration modes. Guidelines on how to predict brake squeal propensity with confidence are yet to be established. In this study, three numerical aspects important for the prediction of brake squeal propensity are examined: how to select an appropriate mesh; comparisons of methods available in ABAQUS 6.8-4 for harmonic forced response analysis; and comparisons of boundary element methods (BEM) for acoustic radiation calculations in LMS VL Acoustics and ESI VA. In the mesh study, results indicate that the mesh has to be sufficiently fine to predict mesh independent unstable modes. While linear and quadratic tetrahedral elements offer the best option in meshing more realistic structures, only quadratic tetrahedral elements should be used for solutions to be mesh independent. Otherwise, linear hexahedral elements represent an alternative but are not as easy to apply to complex structures. In the forced response study, the modal, subspace and direct steady-state response analysis in ABAQUS are compared to each other with the FRF synthesis case in LMS/VL Acoustics. Results show that only the direct method can take into account friction effects fully. In the numerical analysis with acoustic boundary elements, the following methods are compared in terms of performance and accuracy for a model of a sphere, a cat's eye radiator, a pad-on-plate and a pad-on-disc model: a plane wave approximation, LMS's direct (DBEM) & indirect BEM (IBEM), LMS's indirect fast multipole BEM (IFMM) and fast multipole BEM with Burton Miller (DFMM) implemented in ESI/VAOne. The results suggest that for a full brake system, the plane wave approximation or ESI's DFMM are suitable candidates.

## INTRODUCTION

Disc brake squeal is of major concern to the automotive industry as well as customers. It appears in the audible frequency range above kHz [1, 2]. Below 1kHz, structure-borne noises are dominant, as in brake moan and groan, but airborne noises such as brake judder [3] are also present. Low-frequency squeal is defined as noise which occurs below 5kHz and below the first rotor-in-plane mode while high-frequency squeal usually appears above 5kHz [4]. The most comprehensive review papers on brake squeal are: Kinkaïd et al. [1] which covers analytical, numerical and experimental methods, including squeal mechanisms discovered; the work by Akay [2] which discusses the contact problem and friction-induced noise; and the contribution made by Ouyang et al. [5] where the advantages and limitations of the complex eigenvalue method and the transient time domain analysis using the finite element method are presented. Other literature reviews have been written by [6] and, more recently, [7] and [8] which discuss various methods for analysing brake squeal including probabilistic methods to incorporate uncertainties and their implications for practical industry applications. The theory and application of numerical methods in acoustics and their developments have been reviewed by Marburg and Nolte [9]. An excellent comparison between the acoustic finite element method (FEM) and the acoustic boundary element method (BEM) is presented in [10]. In Thompson [11] and Harari [12], the focus is rather on the time-harmonic acoustic FEM. A good book on the acoustic BEM is written by Wu [13] and it explains the direct (exterior, interior) boundary element method (DBEM) and indirect boundary element methods (IBEM), including the collocation method, Galerkin approach) together with ready to use 2D/3D BE code using a continuous element formulation. In contrast, discontinuous elements where the FE nodes are not congruent with the BE nodes, can have some advantages and have been investigated in [14]. In the past, methods for analysing

and predicting disc brake squeal have been focussed predominantly on analytical models to consider some fundamental friction-induced mechanisms and numerical methods for analysis of vibration modes in the frequency domain. Interestingly, the FE time-domain method has mostly been neglected due to its high computational cost and the numerical prediction of acoustic radiation has largely been ignored as only the radiation of brake rotors [15] or simplified annular discs [16–19] have been analysed in the absence of friction. Only recently, an analysis was presented in which the FEM was used to calculate the unstable vibration modes by means of the complex eigenvalue analysis (CEA) and the BEM was used to determine the acoustic radiation [20].

The aim of this paper is, therefore, to introduce the acoustic BEM to predict disc brake squeal in order to complement existing knowledge focussed on structural analysis of FEM models by means of CEA [21]. The finite element methods for structural analysis and boundary element methods for acoustic analysis and the commercial software in which these methods are implemented are given in Table 1. Figure 1 depicts the four models used in this study for performance testing (in terms of their accuracy and computer running times): a sphere, a cat's eye radiator [22], a pad-on-plate model and a simplified brake system in the form of a pad-on-disc system [20]. Two different contact formulations available in ABAQUS are studied, specifically investigating the contact openings between the pad and the disc. A mesh study using tetrahedral and hexahedral elements for the simplified brake system (pad-on-disc model) is undertaken to explore the convergence behaviour of unstable vibration modes calculated by the CEA available in ABAQUS 6.8-4. In Figure 1 (d), tetrahedral elements are shown. Then after a suitable mesh is chosen for structural FE analysis, a method for generating surface velocities for subsequent acoustic radiation calculations using BEM is selected by examining the forced response of pad-on-plate/-disc

systems obtained from the modal, the subspace projection and direct steady-state method available in ABAQUS 6.8-4. This is fol-

Table 1: Software and treatment of non-uniqueness/internal resonance problem (*CHIEF (C)*, *Impedance (I)*, *Burton-Miller (BM)*)

FE-Software				
Method (X)	Modal	Subspace	Direct	
ABAQUS 6.8-4	X	X	X	
BE-Software				
Method (◇)	Direct	Indirect	Fast Multipole	ERP
LMS/VL 8B	◇C	◇I	◇I	◇
ESI/VAOne 2009			◇B	
AKUSTA	◇B			

lowed by a comparison of the acoustic power calculations for the sphere, the cat's eye radiator, and the pad-on-plate/-disc models using the commercial BE tools of LMS/VL Acoustics and ESI/VA (FMM) and the code AKUSTA developed at the Technical University Dresden. Firstly, the sphere and the cat's eye radiator are used to evaluate the performance of acoustic BE codes in terms of how capable and suitable different methods are for overcoming the non-uniqueness/internal resonance problem [9]. Secondly, for the pad-on-plate/disc model, the numerical effect on acoustic calculations of having two bodies in direct contact or by using a wrapping mesh is studied. The effect on acoustic radiation of a possible lift-off of the pad due to contact variations and the application of chamfers is studied to determine the possibility of a horn effect. Based on the results presented in terms of accuracy and computing times required, recommendations for developing a FE/BE model to analyse disc brake squeal are given. For both the structural and acoustic studies, a Hewlett Packard HP xw4600 workstation with an INTEL Q6600 quad core CPU, 8GB of RAM and Windows Vista 64-bit is used to run all simulations.

## MODEL DESCRIPTIONS

The four models used in this study (Figure 1) and described below.

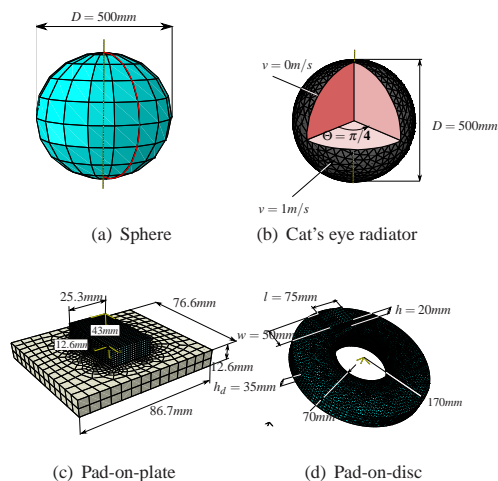


Figure 1: Test cases: (a) Sphere; (b) Cat's eye radiator; (c) Isotropic pad-on-plate; and (d) Isotropic pad-on-disc

**Sphere** The sphere is used as a test case for the non-uniqueness problem in acoustic analysis [23, 24, 9] in order to validate how the direct boundary element method (DBEM) using CHIEF points and the indirect boundary element method (IBEM) using an impedance, are able to overcome the non-uniqueness/internal resonance problem. It is a simple structure in the form of a monopole radiator with an imposed surface velocity of 1m/s. The material properties of the sphere can be arbitrarily chosen, as the surface velocity is imposed on the structural mesh, without having generated surface velocities in a forced response case. The sphere has 96 hexahedral plus 12 tetrahedral elements with a diameter of 0.5m. In LMS/VL a surface mesh consisting of 204 quadrilateral elements is generated which corresponds to more than 6 elements/wavelength at 3kHz. The results us-

ing the DBEM and the IBEM of LMS/VL Acoustics are compared with those from the analytical solution of this model.

**Cat's Eye (Benchmark  $\mathcal{A}$ )** The second model is a cat's eye, as investigated in [25] based on that of [9], which serves as the first performance benchmark model ( $\mathcal{A}$ ). The cat's eye's spherical surface consists of a one octant cut-out, as shown in Figure 1(b). The spherical surface has a velocity boundary condition of 1m/s imposed whereas the element faces of the cut-out octant obtains zero velocity. As in the case of the sphere, arbitrary material properties can be chosen. The solid structure has 8129 linear tetrahedral and the surface mesh has 973 triangular elements. The characteristic length of the elements, is 3cm which corresponds to at least 6 elements per wavelength below 2kHz and at least 4 elements per wavelength up to 3kHz [26]. Four to six elements is recommended practice [27] but for complex geometries at shorter wavelengths and lower order elements, it is recommended to take 10 or more elements per wavelength [28]. For the DBEM, 480 CHIEF points are applied. The diameter of the sphere is reduced from 1m (see [9]) to 0.5m and the frequency range is increased from 1.5kHz to 3kHz. Here, the focus is on calculating the acoustic power as a global measure whereas, in [9], the sound pressure at some locations in the fluid was calculated.

**Pad-on-plate** The pad-on-plate model, as shown in Figure 1(c), is a simplification of the pad-on-disc model: a plate structure (a) does not give any splitting modes; (b) requires shorter run times because the matrices have smaller bandwidths than annular structures; (c) fewer elements are required over a (d) smaller frequency range (2.5 – 6.5kHz instead of 1 – 7kHz). It is a minimalist structure with imposed contact and friction and is, therefore, often encountered as a benchmark model in studies of analytical friction oscillators [29]. Here, the pad-on-plate model serves as a bridge to a simplified brake system composed of one pad in contact with a disc. Young's modulus, Poisson's ratio and density of the plate/pad are assumed to be 210/180GPa, 0.305/0.300 and 7743.8/8024.78kg/m<sup>3</sup>, respectively. In total, 6312 hexahedral C3D8I elements, with incompatible modes properties for improved bending behaviour (incompatible deformation modes are added internally to the elements which increase the degrees of freedom from 8 to 13), are used for the structural analysis, resulting in 4198 quadrilateral acoustic elements. The acoustic elements are surface elements forming the acoustic mesh and do not necessarily have the same coincident nodes as the structural mesh [14]. The boundary element mesh consists of 4198 (LMS/VL) or 4523 (ESI/VAOne) triangular elements, respectively with a minimum of 10 elements per wavelength for a frequency up to 6.5kHz. The plate moves with 1m/s in the  $x$ - direction (Figure 1), with  $p = 1$ kPa applied to the pad.

**Pad-on-disc (Benchmark  $\mathcal{B}$ )** The annular disc (case iron) in contact with a steel pad serves as a second benchmark model ( $\mathcal{B}$ ) for the validation of various numerical models for the purpose of analysing disc brake squeal (Figure 1(d)). Young's modulus, Poisson's ratio and density of the disc/pad are 110/210GPa, 0.28/0.30 and 7800/7200kg/m<sup>3</sup>, respectively. Further, the disc rotates with a velocity of 10rad/s, and a constant pressure of 1000N/m<sup>2</sup> is applied uniformly to the back of the pad. The pad's outer edges are constrained in the  $U_1$  and  $U_2$  directions, which are orthogonal to the disc's plane. The disc's inner edge is constrained in all three global coordinates. As mentioned in [19, 20], an annular disc structure can reproduce major vibration characteristics of a real brake rotor, such as out-of-plane bending motion, which are especially efficient in radiating sound [30]. Unless otherwise mentioned, in structural simulations, the friction coefficient is set to a constant  $\mu = 0.5$  in a finite sliding regime; the pressure  $p = 1$ kPa; and, in acoustic simulations, the speed of sound is set to  $c = 340$ m/s and the fluid's density to  $\rho = 1.3$ kg/m<sup>3</sup>.

## MAJOR PARAMETERS TESTED

Four element types, boundary conditions, sliding definition and contact for structural vibration analysis implemented in ABAQUS are described here. For more detailed description, see [31, 32].

### Mesh and Element Convergence Study

It is essential that a sufficiently large number of an appropriate element type is used to approximate a structural continuum so that the physical results are mesh-independent. Since problems with frictional contact impose a highly non-linear problem, ranging from micro- to macroscopic effects [33, 34], the number of elements in the actual contact zone is a critical factor [32]. Thus the disc and plate have a partitioned area around the contact zone which allows for a locally refined mesh. But, how is the accuracy of complex eigenvalues affected by the mesh quality and element type? Whereas the frequency error due to mesh resolution can be estimated by means of a *normal modes analysis* without considering the instability of the modes, complex mode shapes have to be calculated to explore the convergence behaviour of unstable modes. In this study, 4 element types are assessed: (1) linear tetrahedral fully integrated elements (C3D4); (2) quadratic tetrahedral fully integrated elements (C3D10M) modified to reduce shear/volumetric locking; (3) linear hexahedral reduced integrated elements (C3D8R) with hour-glass control; and (4) linear hexahedral incompatible modes fully integrated elements (C3D8I). Whereas linear and quadratic tetrahedral elements have the advantage of being easier to apply to a real structure, numerical convergence is better for (3) and (4) due to super-convergence points. Quadratic hexahedral 20-node elements, (too costly/difficult to apply to real geometry) are not evaluated.

**Tetrahedral Elements C3D4/C3D10M** C3D4 is a linear, first order fully integrated element. To calculate both stress and displacement values, only one integration point with a constant value is used, but three integration points are used on elements where the pad is loaded. Tetrahedral elements are very stiff, due to their lack of integration points, which is associated with problems of so-called *shear locking* and *volumetric locking* which is a prevalent problem for fully integrated elements. Shear locking gives rise to parasitic stresses. Volumetric locking, due to almost incompressible material properties, occurs only after severe straining of the structure; spurious pressure stresses make the structure too stiff and, in particular, influence bending behaviour, resulting in a smaller number of unstable modes. With a fine mesh, the structure is very stiff and calculated frequencies may lie several hundred Hz above the frequency obtained by using other elements. Moreover, the calculation converges slower than a mesh composed of hexahedral elements due to its lack of super-convergence points [35]. To produce accurate results, the mesh has to be very fine and it has to be ensured that numerical locking is absent. An advantage of tetrahedral elements is that most meshing works well with them when it comes to complex structures like a brake rotor. To overcome the effect of shear and volumetric locking, a 10–node quadratic tetrahedral element (C3D10M) is available; it requires longer computer run times but provides the ease of using the ABAQUS mesher for complicated geometry.

**Hexahedral Elements C3D8R/C3D8I** C3D8R is a linear reduced integrated hexahedral 8–node brick element with second-order accuracy and has fast converging behaviour. Reduced integration Gauss points are BARLOW points [36] which give very accurate strains, calculated as averaged element strains. Reduced integration for hexahedral elements has the advantage that no locking will occur and that the computational costs are much lower due to less integration points used. However, a drawback of reduced integration is that the stiffness matrix is rank-deficient which results in spurious modes due to numerical singularities, so-called *hour-glass modes*. When hour-glassing appears, more modes than usual can be observed, predominantly in the low-frequency regime. C3D8I is a fully integrated linear 8–node brick element, with second-order accuracy and an additional so-called *incompatible modes* property, is applied. The incompatible modes improve bending behaviour due to parasitic shear stresses and prevent *shear and volumetric locking*. If the elements are almost rectangular in shape, their performance approximates the performance of quadratic elements; reduced integration is not necessary and hour-glassing does not appear. However, the computational costs are approximately 3.5 times higher [37], especially for meshes which involve a large number of elements.

### Boundary Conditions

**Constrained Nodes** For the pad’s boundary conditions, all 4 top corner nodes are fixed in-plane but is allowed to move out-of-plane. For the pad-on-disc system, this constraint reduces the frequencies of those modes related to the pad in the range of 0kHz to 7kHz. In this study, models with this type of boundary condition (BC) are called *compliant* (I). Another type of boundary condition for the pad-on-disc system, has the four top corner nodes as well as 10% of the top edges next to the corner nodes constrained such that certain in-plane pad modes are not found below 7kHz, and is referred to as the *stiffened* type. In Figure 2, the results from a mesh with C3D8I elements are depicted. The unstable mode is denoted by  $(m, n, l, q)$ , where  $m$  and  $n$  are the number of out-of-plane nodal circles and diameters respectively and  $l$  and  $q$  are the number of in-plane nodal lines in the radial and tangential directions respectively [17]. In terms of the number of unstable modes predicted, the system with stiffened BC converges faster than that with compliant BC (see Figure 2). For analysis of brake squeal that involves mode-coupling only, stiffened BC is used to eliminate pad modes in the frequency range of interest below 7kHz. For analysis of brake squeal that involves both mode-coupling and pad-mode instabilities [38, 39], compliant BC have to be used. It has been found that stiffer lining materials are more sensitive to changes in stiffness (see also [40]) introduced by alterations in the friction coefficient, the mesh (element type and mesh density) and the material due to the existence of pad modes. Thus meshes for steel linings with compliant BC are studied here. Once the solution for a mesh with stiff lining materials and compliant BC is mesh independent, the BC can be stiffened or softer lining materials can be applied, and the solution will still converge. An investigation of these pad modes, their effects on instabilities and sound radiation will be treated in [38, 39, 41].

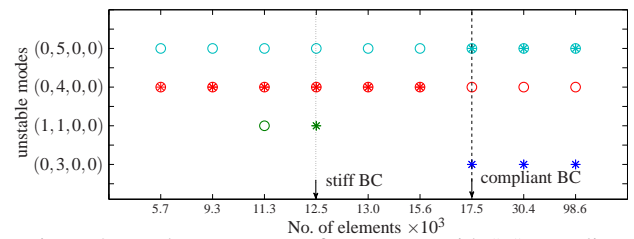


Figure 2: Mesh convergence for systems with "\*" compliant and "o" stiffened boundary conditions. The arrows indicate mesh-convergence for the compliant and stiff boundary condition.

**Contact and Sliding Definition** In this study, *surface-to-surface* contact, (no need of matching meshes) is chosen. The *automatic shrink fit* procedure is enabled to ensure that the two surfaces are in contact before the analysis is run. In Abaqus, as interaction property, for tangential behaviour, the *penalty method* with a constant friction coefficient is used; and, for normal behaviour *hard overclosure*, with allowable separation, is chosen. The penalty method allows for some elastic slip of the two surfaces when they should be sticking [31]. A hard overclosure of the two contacting surfaces allows for limited penetration set here to 0.5mm. Two sliding definitions are available in ABAQUS: the *small* and *finite sliding*. The former is traditionally taken in the CEA as it is not as demanding on computer run times because only relatively little sliding of the surfaces in contact is assumed. The finite sliding allows any arbitrary motion (separation, sliding, rotation) of the surfaces. For the small sliding formulation, the same slave node will interact with the same area (radius of element length) of the master surface throughout the analysis [42]. In the finite sliding formulation, connectivity of the slave nodes to the master surface changes with relative tangential motion. Differences between the two contact algorithms are exemplified in Figure 3. A mesh of 15,665 C3D8R elements with  $\mu \in [0.05, 0.65]$  and stiffened BC is taken. The values of the real part of the complex eigenvalues with small sliding contact are found to be higher than those with finite sliding. It can be observed that the frequencies for the unstable

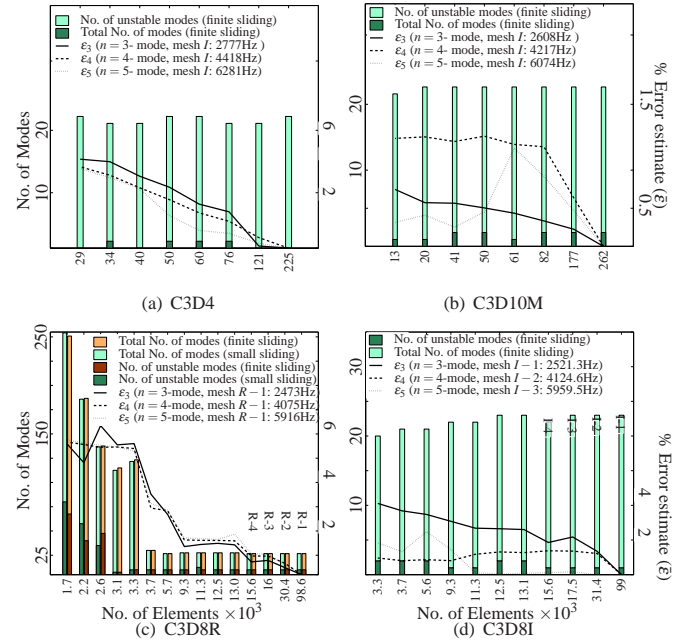
modes with small sliding contact are slightly lower than those with finite sliding and the critical friction coefficients are different.

In Figure 5, the contact opening at around 4060Hz is depicted. The small sliding contact formulation in Figure 5(a) shows for this frequency no lift-off and the contact remained closed. The finite sliding contact condition in Figure 5(b), however, shows much higher deviations of up to 1.5mm; the elements in the contact zone lift up and penetrate and areas without contact appear to have openings of more than a millimetre, illustrating more realistic effects on the structural dynamics. Even though the dynamic effects like the impulse of a lift-off and re-attachment are not modelled with CEA, in the time domain, it represents a very severe discontinuity and a switching mechanism [43]. The effects of acoustic radiation might also be important and will be discussed in a later section.

**Mesh Study**

Firstly, a model of the pad-on-disc system with linear tetrahedral fully integrated elements is used for the mesh study. Secondly, again tetrahedral elements, but with quadratic shape functions (10 nodes) and modified bending behaviour are used. After that, hexahedral 8–node elements with reduced integration and enhanced hour-glass stiffness (see ABAQUS manual 6.8.4 [31]), are studied. Finally, hexahedral ‘incompatible modes’ elements, which allow for better bending behaviour are investigated. For each element type, various meshes are used and the difference in predicted frequencies of three prominent out-of-plane split modes with  $n = 3, 4$  and  $5$  nodal diameters, between a given mesh and the finest mesh is evaluated (normal mode analysis). The total number and the number of unstable modes extracted (complex modes analysis) are also included in Figure 4. For the linear tetrahedral elements (Figure 4 (a)), it is obvious that the number of unstable modes does not converge as the only unstable mode is the  $(0, 5, 0, 0)$ -disc mode which even becomes stable again for a finer mesh. Also, the total number of extracted normal modes alternates between 18 and 19. The smaller the average element size chosen, the more compliant the structure becomes. In Figure 4 (b), quadratic tetrahedral 10-node elements are evaluated for finite sliding contact. The solution converges to two unstable modes, that is, the  $n = 3$  and  $n = 5$  modes. Also, the errors in frequency of the three dominant out-of-plane modes of the disc are significantly lower for coarser mesh compared with those of the linear tetrahedral elements.

even 300 which is due to artificial hour-glassing effects: the mesh is distorted in an uncontrolled way due to zero strain value at the only integration point, resulting in overprediction of modes and an overly compliant mesh. For the finite sliding contact, the number and kind of unstable modes no longer change after a mesh with 5642 elements although, still, hour-glassing can be observed; and, for the small sliding regime, the unstable modes converge only after the 7<sup>th</sup> step. By comparing the number and quality of unstable modes as well as the frequency errors, it can be observed that the number of unstable modes converges for a mesh with total number of at least 6,000 elements for the finite sliding contact and, 11,000 for the small sliding contact, with an error in frequency of less than 3% and 2%, respectively. For the *incompatible modes* elements



force, which transfers its energy through the pad to the contact area of the disc in the form of pressure excitation. On the other hand, for the disc alone, it is directly excited by a concentrated force and an indirect pressure effect is not available. However, the dominant frequencies match, indicating the dominant character of the disc for the pad-on-disc system. Further, the pre-stressed structure behaves similarly to the system with friction and only very small differences in the response with  $\mu = 0.05$  can be observed. Clearly, additional modes, which lie around 2 and 2.2kHz, correspond to pad modes with predominantly in-plane motions. The positions of these modes are determined by (1) boundary conditions (such as contact), (2) material properties and (3) the element type used. Closer analysis

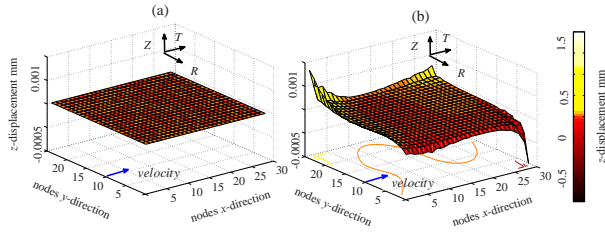


Figure 5: (colour online) Contact opening depicted in coordinates of  $z$ -displacement for (a) small sliding and (b) finite sliding definition for pad-on-disc system with friction coefficient of  $\mu = 0.5$  at frequency of 4059Hz (finest mesh Figure 4(d)).

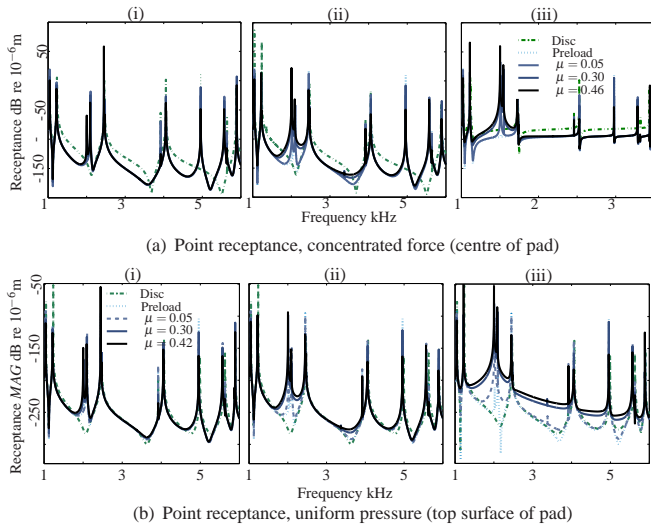


Figure 6: (colour online) Forced response cases: (a) concentrated force on centre node of the pad; and (b) uniform pressure on top surface of the pad for model IV: (i) modal method, (ii) subspace projection method and (iii) direct harmonic response

shows that a pad mode becomes active at 2kHz and 2.2kHz in mostly the radial and tangential directions, respectively. These modes have out-of-plane components coupled with a 'vibrational active' (Chen [44]) (0, 3, 0, 0) disc mode which lies at around 2.39kHz. In [45] by means of a time domain simulation of the same simplified brake system, the pad modes cause higher vibration amplitudes at this frequency, which is not predicted by CEA. For the point receptances (Figure 6), this is also discernible from the disc's response which does not show peaks at these frequencies. Then, when friction is applied, the changes in displacement become visible, especially at frequencies of these pad modes. In the investigation of the surface mobility due to contact area excitation by Dai [46], an additional moment in the contact area is found to be responsible for additional modes which is confirmed here by additional peaks in the point receptance. Further, due to the in-plane character of these modes, feed-in energy due to the self-exciting characteristics maximises and increases the response of the system at these frequencies. This effect is highlighted in the subspace method and the direct harmonic response as these two methods support asymmetrical stiffness effects

due to friction while linear modal solutions are unable to resolve these effects. In Figure 6(b), the structure is analysed by a harmonically varying uniform pressure of 1kN. In order to simulate pressure on the disc alone, the contact area of the pad is partitioned on the disc and pressure is applied to only this region. This time, the disc alone is directly pressurised, the response of the disc alone is comparable in terms of excitation with the forced response of the pad-on-disc system and in general, lower at the dominant frequencies than that of the system with friction. Whereas the modal approach and the subspace projection method do not differ significantly from the concentrated force, the direct steady-state method shows far more obvious differences: a lifting up of the response spectrum is not only observed at frequencies of the pad modes but over the whole bandwidth.

Figure 7(a) displays a comparison of the pad-on-plate's forced response in terms of kinetic energy [38], calculated by the subspace projection method and the direct steady-state response for a pressure of 0.5MPa. The results of the modal method are not included in Figure 7 because it has already been shown in Figure 6 that friction effects are not considered [32] in this method. The four dominant frequencies are indicated by  $f_1$  to  $f_4$ . With an increasing friction coefficient, both the direct steady-state and subspace projection methods show increases in the kinetic energy. Clearly, the effects of friction are underestimated by the subspace projection method, resulting in lower kinetic energy amplitudes. For the subspace projection method, all modes in the frequency range of kHz to 6.5kHz but without residual modes are used. Including modes up to 10kHz improves the behaviour slightly but also results in longer computer run times, thus reducing the advantage it has over the direct calculation approach. Similary Couyedras et al. found by means of a comparison of the direct time integration with the constrained harmonic balance method, that many more harmonics are necessary to receive the steady state nonlinear solutions for a brake system [47]. In Figure 7(b), the development of external work, which includes work due to all external forcing terms and friction, calculated by the subspace projection method is depicted for friction coefficients from 0.05 to 0.65, together with the direct steady-state method for  $\mu = 0.05$ . The external work represents the change in potential energy stored in penalty springs due to friction [37]: negative external work increases their spring load which is missing at this frequency to increase the potential energy of the structure due to deformation [48]. However, the external work usually becomes higher at certain frequencies with increasing external loads and only when energy due to friction-induced excitation is fed into the system can the sign of energy be reversed. The storage of potential energy is proportional to feed-in energy. Increased feed-in energy is only visible at frequencies of  $f_2$  to  $f_4$  at which the feed-in energy for the direct steady-state analysis is much higher than it is for the subspace projection method. By looking at the reference level (dotted line), one can clearly see that the overall level of external work of the direct steady-state analysis is lower, indicating that more energy is fed into the system thus lowering contributions due to external work.

## ACOUSTIC RADIATION

For the evaluation of the acoustic radiation problem, various methods are assessed. For that, in LMS/VL Acoustics [49] the integrations in are set to region limits of  $D/L$  in the range of integer values or 0 to 5 for the near- and far-fields respectively. Here  $D$  is the distance between two boundary elements and  $L$  is the longest edge. The quadrature is set to 5, 3, 1 for the near, medium and far regions, respectively, with up to 100 Gauss points. In AKUSTA, the Gauss quadrature order is set to {2, 4, 6, 8, 12, 16, 24, 30; 30} which is lower than in LMS, as a polynomial transformation is implemented, which allows to reduces significantly computational cost due to integration with at the same time higher accuracy [50]. The convergence criterion for the fast multipole solvers in LMS and ESI have been set to as  $5.5 \times 10^{-4}$ , after an integration convergence study at some arbitrarily chosen resonance frequencies.

## Numerical Methods used in Acoustic Simulations

Numerical methods suitable for exterior acoustics are assessed using the models depicted in Figure 1.

**Analytical Sphere** A sphere as a test object represents simple geometry which can show irregular frequencies/internal resonances for external acoustic radiation calculations. For that purpose, an analytical closed solution for the sound pressure,  $p(R) = \frac{\rho c v k R}{\sqrt{1+k^2 R^2}}$  as a function of the wavenumber was taken from [51]. Here,  $\rho = 1.3\text{kg/m}^3$ ,  $c = 340\text{m/s}$ ,  $v = 1\text{m/s}$ ,  $R = 0.25\text{m}$  and  $k = \omega/c \in [6.28, 18.48]$  are the fluid's density, the sonic velocity, the velocity in the normal direction applied to each node, the radius of the sphere, the wavenumber and circular frequency respectively.

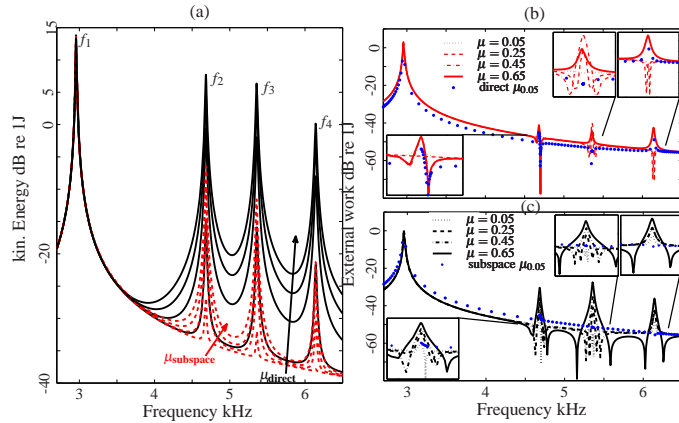


Figure 7: (colour online) Comparison of subspace projection method and direct steady-state analysis: (a) kinetic energy; (b) external work *subspace projection method*; and (c) external work *direct steady-state analysis* ( $p = 0.5\text{MPa}$ ,  $\mu = 0.05$ )

**ERP (LMS/VL)** The method of equivalent radiated power (ERP) implemented in LMS VL (Virtual Lab Acoustics), as a plane-wave approximation, sets the radiation efficiency  $\sigma$  to 1 so that the acoustic power  $\Pi$  in the far-field is calculated by taking only the surface velocity into account. The typical BE matrices do not have to be assembled and reflections are not considered in the solution of acoustic power. An integration error, due to calculating the pressure of two contacting surfaces, is not expected because the pressure is not calculated by setting up and solving the BE matrices. The acoustic power is directly calculated by equating  $1 = \sigma = \frac{\Pi}{\rho c S \langle v^2 \rangle}$ . Here,  $\rho$  is the fluid's density,  $c$  is the speed of sound,  $S$  is the radiating surface and  $\langle v^2 \rangle$  is the time and space averaged surface velocity [26].

**Direct BEM (DBEM) of LMS/VL** Direct boundary element formulations work by directly solving the Kirchhoff-Helmholtz equation [52] through discretising the surface and then using for instance the collocation method [53]. The interior of the volume of the radiating body is not described mathematically and, in the frequency spectrum *irregular frequencies* (non-uniqueness problem) can be observed. These frequencies are physically not explained as they are only mathematical artefacts [9]. To overcome the problem, the system of equations can be enlarged by overdetermination points which are placed inside the volume of the radiating body. The major drawback of this method is that, as the geometry becomes complicated [9], the exact location of these over determination points inside the volume of the radiating body is no longer known so that more points than necessary have to be applied, each of them increasing the system matrices by one dimension.

**Indirect BEM (IBEM) of LMS/VL** This method is based on the solution of the exterior and interior acoustic radiation by means of a Galerkin approach [13]. As the interior is mathematically described in this model, the previously described non-uniqueness problem becomes physical and can be described by internal resonances. If one

wants to use the indirect method in order to calculate only the exterior acoustics, the internal effects of the radiating body have to be eliminated. This is usually done by applying a layer of characteristic impedances, inside the volume. For air, the characteristic impedance is  $Z = 10^{-3}\text{Nsm}^{-3}$ .

**DBEM/Burton-Miller (BM)** AKUSTA, developed at the technical university of Dresden is able to use, besides other methods, the Burton-Miller approach, which treats irregular frequencies due to mathematical singularities (opposed to physical/ geometrical singularities [54]), by forming a linear combination of matrices of the discretised Kirchhoff-Helmholtz equation with its second derivatives and a weighting function, the Burton-Miller constant [52, 55]. In order to have defined second derivatives at the nodes of the BE mesh for additional integrands of the Burton-Miller components, nodes of the BE mesh have to be  $C^1$  continuous. This means that unique derivatives have to exist; this is not the case, if a continuous element formulation as in FEM is chosen. Practically, this can be solved by using a discontinuous element formulation [56, 57]).

**(indirect) Fast Multi-pole BEM (IFMM) of LMS/VL** Fast multipole solvers work by means of substructuring the fluid domain into levels of cluster trees (or sub-domains) and subsequent approximate solution at these levels [58, 9]. The IFMM has some restrictions (see also [59]) due to this substructuring process. The length of level zero is the maximum length of the geometric body which is, in the case of the cat's eye radiator, the diameter of 0.5m. This cube is divided into  $8^N$  cubes with  $N$  being the level counter, so that, for level one, there are 8 sub-domains created. The length of the  $N^{\text{th}}$  cube is calculated by  $L_N = L_0/2^N \leq \frac{\lambda}{4}$  where  $\lambda$  is the shortest wavelength with 11.3cm for a sonic velocity of 340m/s at a frequency of 3kHz. Hence, the number of levels is 2.88, that is, 3 and there are 512 sub-domains. The IFMM far-field approximations can only be used when the cubes are not adjacent, that is, only cubes at the minimum level, 2, can be calculated by the ACTIFMM solver while, for the rest, the classic SYNOISE solver is used. It is expected that the solution of the IFMM is the most reliable in the frequency interval of 607Hz to 2000Hz. The advantage of the fast multipole in general is, that it substructures and solves for the acoustic domain in a heuristic manner and uses only a fraction of the computer memory even for very large models. Further, due to the use of approximations, especially at high frequencies, the computer run times are supposed to be much lower. As a result, model sizes with up to 1Mio. dof's can be solved [60].

**(direct) Fast Multi-pole BEM (DFMM) of ESI/VAOne** The second fast multi-pole solver, implemented in ESI VAOne, is based on previous pre-conditioning and subsequent iterative solving with a flexible Generalized Minimal Residual Method (fGMRES), treating irregular frequencies by means of the Burton-Miller Method [61]. In contrast to the Burton-Miller method implemented in AKUSTA, the element formulation is continuous and the regularisation of the integrals is based on an approximation. However, in this study, no irregular frequencies in the acoustic power or pressure could be found which means, that the BM approach used is working fine, although the elements are not  $C^1$  continuous.

## Irregular Frequencies/ Internal Resonances

For external acoustics based on a direct formulation, the irregular frequencies are not physical as the interior of the volume is not governed by its underlying integral equations. For the direct method, CHIEF or the Burton-Miller approach can be chosen to overcome the so-called non-uniqueness problem [13]. For the indirect methods, radiation modes due to internal resonances can be treated by applying a layer of impedance inside the volume. The first irregular frequency of a cavity can be estimated from  $\frac{c}{2L}$ , where  $L$  and  $c$  are the characteristic length and the speed of sound respectively. For a sphere with diameter,  $D$ , an irregular frequencies may appear for frequencies greater than 340Hz. The same can be assumed for the cat's eye, as it is derived from the sphere with similar dimensions. However, more irregular frequencies are expected due to the more complicated geometry [9]. For the plate and disc structures, irregular frequencies/internal resonances are tested using the

acoustic FEM in ABAQUS. The interior of the disc is meshed with quadratic 20–node acoustic brick elements. The outer surfaces are constrained with a zero pressure boundary condition (interior Neumann problem). The bulk modulus of elasticity of the fluid air is set to  $K = 150,280\text{Pa}$ , the density is assumed to be  $\rho_f = 1.3\text{kg/m}^3$  and the speed of sound is  $c = 340\text{m/s}$ . The first irregular frequency for a plate of thickness of 12.6mm is calculated at 13,863Hz (see Figure 8(a)). By using  $\frac{c}{2T}$ , the first irregular frequency is estimated to be above 13,493Hz. For the disc, the first fluid’s radiation mode, corresponding to an irregular frequency of the exterior problem, is found via the acoustic FEM at 5140Hz (estimate 4857Hz which corresponds roughly to a wavelength of 6.5cm (see Figure 8(b)). For the

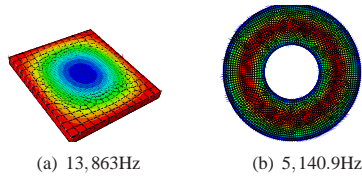


Figure 8: First irregular frequencies of: (a) plate; and (b) disc

pad of the pad-on-disc system, the first irregular frequency appears at around 9041.1Hz (estimate 8500Hz), which is out of the range of interest in this study, as only frequencies up to 7kHz are investigated. The pad of the pad-on-plate system showed irregular frequencies at around 14kHz.

**Test for Irregular/Internal Frequencies**

**Sphere** The acoustic radiation of a sphere is calculated using the direct exterior BEM and the IBEM, both of which are available in LMS/VL Acoustics. The direct method is calculated once without CHIEF points and, in the second run, 480 over determination points are applied, similar as in [22]. The indirect method calculates the interior and exterior problems at the same time. In order to eliminate the effect of interior resonances, an absorbing interior panel, with a characteristic impedance of air of  $Z = 10^{-3}\text{Nsm}^{-3}$ , is applied [26]. As can be seen in Figure 9, the DBEM shows the effect

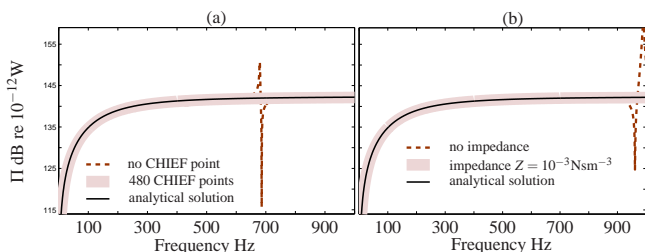


Figure 9: (colour online) (a) DBEM and (b) IBEM applied to radiating sphere

of irregular frequencies on the acoustic power at 680Hz, while the indirect method gives an internal resonance at 961Hz. By applying (a) overdetermination points or in (b) a layer of impedance on the interior of the sphere’s surface, both methods work well: a comparison with the analytical solution shows no differences. This simple example also shows that irregular frequencies are not identical to internal resonances as the integral equations involved are different and that CHIEF points or the characteristic impedance overcome the non-uniqueness/internal resonance problem.

**Cat’s Eye (Benchmark  $\mathcal{A}$ )** Next the cat’s eye radiation properties are studied in terms of acoustic power. The performance in terms of irregular frequencies/internal resonances of various acoustic BE formulations suitable for analysis of disc brake squeal is analysed. It is interesting to determine whether some methods can be excluded by examining the acoustic power ( $\Pi$ ) as a global measure alone. Then, selected methods are assessed in terms of their performance to analyse the acoustic pressure at the centre and backside points of the spherical part [9]. In Figure 10, the different methods are compared

with each other. If the acoustic power  $\Pi$  is expressed in dB, almost no difference can be seen for frequencies above about 750 Hz. The IFMM follows the IBEM very closely as it is based on the same formulation. Here, for frequencies between 250 and 750Hz, these indirect methods seem to over-predict the acoustic power compared with the other methods. As can be observed in the magnification of Figure 10, the DBEM/CHIEF also suffers from the effects of irregular frequencies, especially at higher frequencies, which simply means that more CHIEF points have to be applied. All methods show that  $\Pi$  approximates the ERP method very closely. The DBEM/BM (AKUSTA) and the DFMM of ESI’s VAOne both working with Burton-Miller formulation do not show any irregularities and are relatively easy to apply. Figure 11 depicts the sound pressures in the centre and back of the cat’s eye for these two methods working with the Burton-Miller approach. The sound pressure is generally more sensitive than acoustic power to the effects of irregular frequencies due to singularities. In the center of the cat’s eye, the sound pressure diverges very strongly for the fast multipole method. The differences at the center node are probably due to (1) the continuous element formulation of the DFMM which is different from the constant discontinuous elements used in DBEM/BM (AKUSTA) which is  $C^1$  continuous [62] and (2) the different choice of the Burton-Miller coupling parameter which was chosen to be 0.1 as a compromise between performance and accuracy for the DFMM according to [61] and the optimal choice of 1 [55] in AKUSTA. Important here is, that the divergent behaviour at the center node is expected and that for both methods, the DFMM of ESI and the DBEM/BM (AKUSTA), work well for approximating the sound pressure at the back of the cat’s eye surface with a smooth function to that of a sphere. The behaviour of the center node is related to the character of this geometric singularity at which the effect of irregular frequencies gets amplified [22] and which can get remedied by different mapping approaches [54], which however, is beyond the scope of the paper.

**Test for Integration Error in Contact Patch**

For a pad-on-disc or the pad-on-plate in which two bodies are in frictional contact, it is likely that integration errors in the contact surfaces influence  $\Pi$ . The significance of integration errors is dependent on the method used but can be circumvented by wrapping the pad and disc with one additional mesh, together with subsequent mapping of the surface velocities onto this new mesh.

**Pad-on-plate** In Figure 12, the significance of different sliding regimes and a possible integration error due to the contact surfaces is evaluated for the pad-on-plate model. The DBEM, which supposedly has additional integration errors due to the contacting surfaces, but also considers reflection due to geometry, is compared with the ERP, in which the integration error of the BEM is minimised because the surface pressure and also reflections are not calculated. In

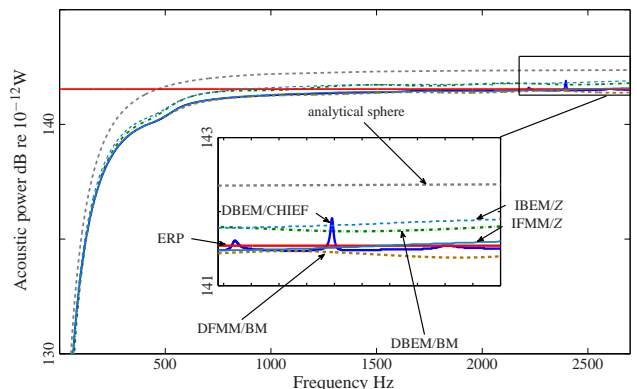


Figure 10: (colour online) Acoustic power levels of cat’s eye for various numerical methods

Figure 12(a), the acoustic power level  $\Pi$  of the ERP method is depicted for both the small ( $\Pi_s^p$ ) and finite sliding ( $\Pi_f^p$ ) regimes and

almost no differences can be observed. There is also no difference between the acoustic power level for the small and the finite sliding contact using direct BEM, indicated by  $\Pi_s^d$  and  $\Pi_f^d$ . In Figure 12(b), two curves show the difference in acoustic power expressed in % based on Watts, between small and finite sliding for both the DBEM ( $\Delta_{Direct}$ ) and the ERP ( $\Delta_{ERP}$ ) method.  $\Delta_{Direct}$  represents a measure for the integration error, reflections and differences in the sliding regimes while  $\Delta_{ERP}$  only gives a measure for differences in the sliding regimes plus an overestimation due to the use of ERP which is supposed to be rather small for the high-frequency range [9]. Differences of up to 13% can be observed for both the DBEM and the ERP which are almost congruent, indicating that, an integration error is rather small. In Figure 12(c),  $\Delta_{Direct}$  is deducted from  $\Delta_{ERP}$  and depicted in %. The differences do not exceed 2%, thus indicating that the effects of reflection plus integration error are very small compared with the effects due to different sliding definitions. That the effects of reflection are small for the pad-on-plate system has previously been shown in [25] where energy area contributions do not show major differences compared to acoustic intensity. It has

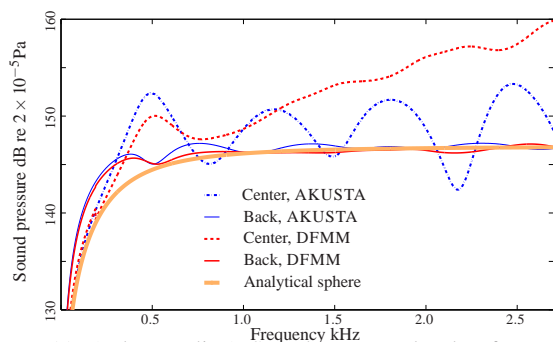


Figure 11: (colour online) Sound pressure levels of DBEM and DFMM, both using Burton-Miller approach

to be noted that a possible lift-off of the pad, as depicted in Figure 5, is not applied to the BE methods with regard to the reflections as the structural mesh was taken in its undeformed state from the FE analysis. For the plate or disc models it can be stated, that DBEM can be used *without* considering a wrapping mesh. However, for a real brake system in order to circumvent any problems associated with an additional integration error, a wrapping mesh is recommended.

In Figure 13,  $\Pi$  is calculated by the ERP, the DBEM (no CHIEF points, as no irregular frequencies are expected at this low frequency) and the DFMM for the pad-on-disc model. The last approach is used in calculations for three different wrapping meshes which have (i) 2,551 nodes (2.67mm EL), (ii) 6,952 nodes (1.63mm EL) and (iii) 23,022 nodes (0.905mm EL). *EL* is the *desired element length*, which should correspond to at least 6 elements per wavelength. This element length is not to be confused with the *average characteristic length* in the contact zone defined by ABAQUS. The former is homogeneously distributed over the surface and does not consider the partitioned contact area. The contact area was seeded and meshed, with an element length of 1.63mm in the contact partition and as can be seen from Figure 13, exactly the same desired element length has to be applied to the wrapping mesh in order to obtain results which match the non-wrapped structure of DBEM and DFMM with the ERP as upper bound, as this method overestimates the acoustic power [9]. When no wrapping mesh is applied, the results do not deviate greatly from the results of the LMS/VL Acoustics DBEM and the medium-sized wrap with an *EL* of 1.63 mm which is as small as the element size in the contact zone.

**Pad-on-disc (Benchmark  $\mathcal{B}$ )** In order to use the DBEM for the pad-on-disc system, overdetermination points, have to be applied. Care has to be taken that these points are only applied to the interior of the disc and that no points lie *in the contact patch or pad volume*. If this is guaranteed, an overdetermination study can be performed for which the acoustic power level should converge (see Figure 11). As a more strict convergence criterion, the sound pressure

at (arbitrarily) chosen field points can also be specified (as exemplified in Figure 11). Ideally, the convergence has to be checked at as many frequencies as possible; however, as this is not feasible, it is suggested to choose frequencies corresponding to prominent disc modes. In Figure 14, an overdetermination point convergence study is presented for the pad-on-disc model, here for the disc's first three out-of-plane modes. It has been found that convergence is reached if at least 3000 overdetermination points are applied (see Figure 14), so that 3500 overdetermination points were taken.

Next shown in Figure 15 is the radiated acoustic power for different calculation methods for the pad-on-disc model. The IBEM and IFMM, have characteristic impedances of  $Z = 10^{-3} \text{Nsm}^{-3}$  (air) applied. The DBEM/BM (AKUSTA) does not converge fast enough and no results are presented here. Only for ESI/VAOne's DFMM, both a wrapped and a non-wrapped structure are calculated but there are insignificant differences between the two. All methods appear to work well and the modes which contribute most to the overall sound radiation are able to be identified and no method can be excluded. However, by zooming in (magnifications  $A_1 - A_4$ ), differences in the methods can be distinguished, but are not significant for this pad-on-disc system. However, one has to bear in mind, that with higher geometric complexity and more parts, the modal density increases, so that stronger irregularities due to integration errors or the non-uniqueness/internal resonance problem are potential sources of misinterpretation. At around 2kHz, the IFMM shows a peak which does not correspond to a regular frequency. More exposed peaks lie at frequencies of around 3.3kHz and, at around 4.2kHz and the IBEM is not smooth. Integration errors are present in  $A_1$  to  $A_3$  which are associated with not using a wrapping mesh because irregular frequencies/internal resonances are only found above 5.1kHz. Above 5kHz, the irregularities of the DFFM without wrapping are due to integration errors as the curve of the wrapped structure is smooth.

### Computational Costs

Not only performance but also computational costs are important. As all models used in numerical simulations represent only approximations, it is the trade-off between accuracy (physically meaningful) and computational cost (feasibility) that determines the practicability of the method to be employed. Therefore, the computing times required to calculate the sound pressure from the surface velocity and then the acoustic power are compared in Figure 16 for the various methods. All simulations used in-core solvers and no other major process ran on the workstation. The main advantage of the fast multipole formulations (DFFM, IFFM) is that their memory usage is less than those of the non-heuristic methods, such that it becomes feasible to analyse large models. This could be particularly important for simulating a full brake system. As can be seen in Figure 16(a) for the cat's eye radiator, the DBEM with Burton-Miller and the IFMM do not offer significant advantages in terms of computational cost. In Figure 16 the performance of codes in numerical acoustics is presented in terms of normalised time/frequency for (a) the cat's eye model ( $\mathcal{A}$ ) and in (b) for the pad-on-disc system ( $\mathcal{B}$ ). For the cat's eye model, the performance of AKUSTA is significantly lower than that of the commercial codes. This is because the parallel use of multiple processors for one step is not possible. The IFMM does not perform well as the model size of the cat's eye radiator is far too small. The IBEM performs much faster. However, for the indirect method, the internal resonance frequencies remain problematic so that here the impedance of water is better used. The DBEM performs well, provided that enough overdetermination points (CHIEF) are properly assigned to the structure. The DFMM is slower than the DBEM or the IBEM but its performance is convincing for the cat's eye radiator. Although the DBEM and the IBEM of LMS/VL perform well, here the preference is for the DBEM as the IBEM suffers from larger errors, due to either internal resonances still being present regardless of an applied impedance or due to integration errors. The major disadvantage of the DBEM is the large memory consumption which gets even worse when CHIEF points have to be applied, rendering this method as non-applicable for large models.

A second benchmark, with its focus being on not having a wrapping mesh applied, is performed on the pad-on-disc model ( $\mathcal{B}$ ). Due to the non-matching meshes in the contact zone, integration of the methods using the DBEM/BM approach suffer; this could be observed in the very slow convergence rates of the iterative generalized minimal residual method (GmRes). The performance of iterative solvers can be found in [14]. The convergence rate of the DBEM/BM (AKUSTA) is too low and calculations were prematurely aborted for the pad-on-disc model. For the DFMM, two calculations are depicted in Figure 16(b). The large bar gives the average times/frequencies for a structure without wrapping mesh and highlights the problems the Burton-Miller approaches have with the contacting surfaces. However, the application of a wrapping mesh speeds up calculations considerably due to a faster convergence rate of the iterative solver and, at the same time, has very low memory consumption (small bar). Thus the DFMM method implemented in ESI VAOne with a wrapping mesh is recommended for future calculations of a real brake system as it combines accuracy and ease of handling due to the Burton-Miller approach and fast calculations with low memory consumption from  $kD$  of 0.0025 up to  $kD$  of 250 (which is going to be increased up to  $kD = 500$  in VAOne 2010), where  $k$  is the wavenumber and  $D$  is the diameter of the acoustic domain.

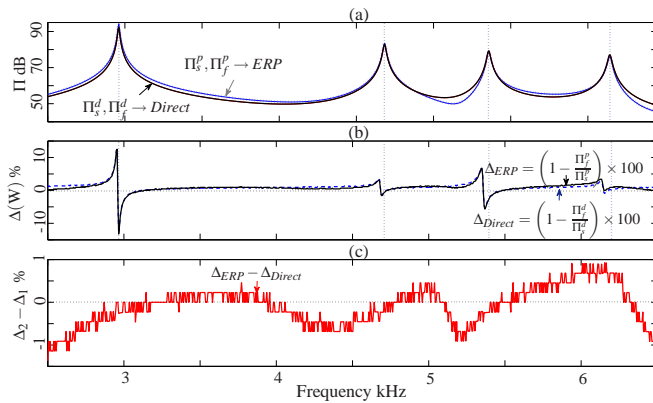


Figure 12: (color online) (a) Acoustic power for DBEM and plane-wave approximation (superscripts  $d$  and  $p$ ) for small and finite sliding regimes (sub-scripts  $s$  and  $f$ ); (b)  $\Delta_{ERP}$  and  $\Delta_{Direct}$  of acoustic power in  $W$ ; (c)  $\Delta_{ERP} - \Delta_{Direct}$

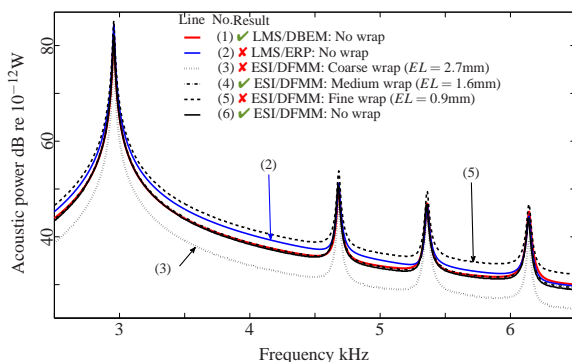


Figure 13: (colour online) Acoustic power levels of pad-on-plate model for different wrapping meshes ( $\mu = 0.05$ ,  $p = 1kPa$ )

### Possible Consequences of Pad Lift-off and Chamfers

As there are cavities, due not only to contact patch deformations and lift-offs (Figure 5) but also naturally to the different geometries (form factors  $FF$ ) of the pads, a possible gap between disc and pad is studied. In this parametric study at 4060Hz, the pad is lifted off the disc, starting from 0mm (in contact) over 0.5mm and then in 1mm steps up to 7mm, using the DFMM solver of ESI. Only the finite sliding contact algorithm in ABAQUS is taken and the field-point mesh is evaluated at 1m distances. Figure 17(a) shows a (distorted) dipole

[51]. In Figure 17(b), the shape of a lateral quadrupole [51] can be discerned which becomes clearer for a contact opening of 0.5mm. Leaving a gap between the disc and the pad results in a horn effect with significant amplification, a well-known phenomenon, and leads also to undesired sound pressures in for instance tyre-road-contact noise calculations [63]. Of course, due only to different contact regimes, it is not very likely that the pad lifts off at 7mm; thus, this scenario has to be seen as hypothetical. However, due to a real

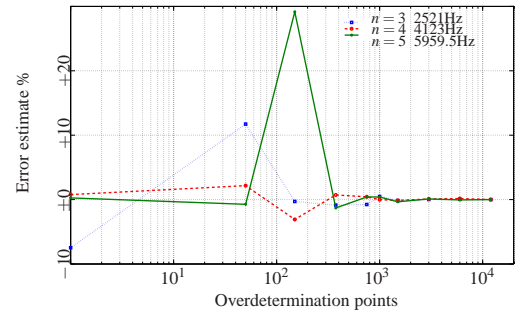


Figure 14: Error estimate in acoustic power relative to finest acoustic mesh ( $R - 1$  Figure 4(c)) and acoustic power of three out-of-plane modes

pad having slots and chamfers, it is suggested in the next step that the pad's form factor be modified. Four cases are depicted in Figure 18: (Case I) baseline configuration with steel pad and a compliant BC; (Case II) Case I with chamfers and a compliant BC; (Case III) Case I with chamfers and stiffened BC; and (Case IV) Case I with chamfers and stiffened boundary conditions such that the weights of pad (I) and pad (IV) are equal. For case I the  $(0, 4 \pm, 0, 0)$  mode becomes unstable. For case II, due to its higher mass and less rigid boundary conditions, pad modes, previously at around 4.72 – 4.82kHz, now appear at 3.1kHz. For this case, the  $(0, 4 \pm, 0, 0)$  split mode becomes stable and the  $(0, 3 \pm, 0, 0)$  mode at around 2500Hz is unstable. In order to maintain the same unstable modes for all 4 cases, the lining material is changed (density) and the boundary conditions are altered to constrain more nodes. Again, the  $(0, 4 \pm, 0, 0)$  mode becomes unstable, with pad modes lying at around 4.75 and 5.56kHz. In the upper right corner of Figure 19(b), the acoustic power level,  $\Pi$ , for Cases I-IV is denoted. The results clearly show that the effect of chamfer is to amplify the acoustic pressure. This is disadvantageous and has to be further evaluated to determine if and, if so, by how much, the acoustic pressure is shielded by e.g. the calliper assembly.

## DISCUSSIONS AND CONCLUSIONS

**Boundary Conditions and Mesh Study** It is found that, for stiffened boundary conditions, convergence of the solution, in terms of unstable modes predicted by the CEA, is much faster as pad modes are not found in the frequency range investigated. However, pad modes, vibrating in-plane either radially, tangentially or rotationally, could be unstable and initiate or amplify underlying or neighbouring mode coupling [38]. They are very sensitive to changes in mesh resolution or contact stiffness and influence predictions in terms of the complex eigenvalues: Therefore, a mesh study for converged solutions has to concentrate on a frequency range where pad modes are present. Two contact formulations, small and finite sliding, are studied by means of  $C3D8I$  elements without considering pad modes. The finite sliding contact is stiffer as the frequencies of predicted unstable modes are higher. The critical  $\mu$  predicted is different for the two contact conditions (see Figure 3). The contact patch, of the finite sliding contact shows a lift-off which definitely changes the dynamics and could itself be responsible for higher acoustic radiation. Therefore, the finite sliding regime is recommended as the local surface lift-off is more realistic. Extra calculation time required is so small as to be almost not measurable for the pad-on-disc model. The tetrahedral 4-node and 10-node elements are benchmarked against the 8-node hexahedral elements. The typical drawback of the linear  $C3D4$  becomes obvious since the frequencies of the modes are very high: the structure is far too stiff compared with the other elements. This is related

to the out-of-plane motion where elements lock into each other, also referred to as *shear locking* which is a numerical error and results in sometimes only one mode being predicted to be unstable: The solution is not mesh independent. Therefore, the tetrahedral elements should be avoided and only used to fill ‘gaps’ whenever it is easier to apply tetrahedral elements in the support of the mesh structure [31]. The 10-node tetrahedral element performs better and can be easier meshed. However, it suffers from large computing times as it has many more nodes than the 4-node tetrahedral element and lacks super-convergence. The use of fully integrated hexahedral elements results in large computer running times. Therefore, often the hexahedral *C3D8R* element, is taken. This element type suffers from hour-glassing and serious over-prediction of unstable modes if the mesh is too coarse. The incompatible mode element *C3D8I* produces better results than does the *C3D8R* element and no hour-glassing is observed. The numbers of total modes and unstable modes converge. A drawback is, that for the pad-on-disc system, the computer run times are more than 4 times larger than that for *C3D8R*.

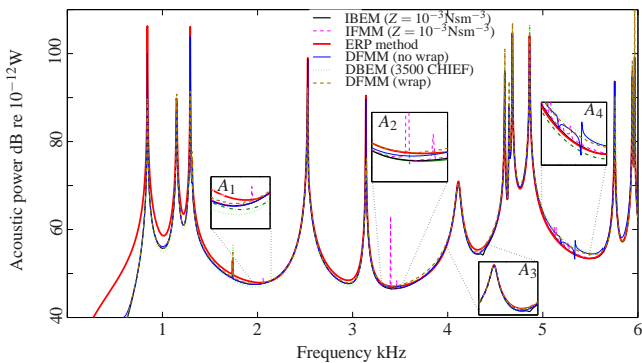


Figure 15: (colour online) Acoustic power levels for pad-on-disc system for methods implemented in LMS/VL: IBEM; IFMM; ERP; DBEM and for the DFMM solver implemented in ESI/VAOne

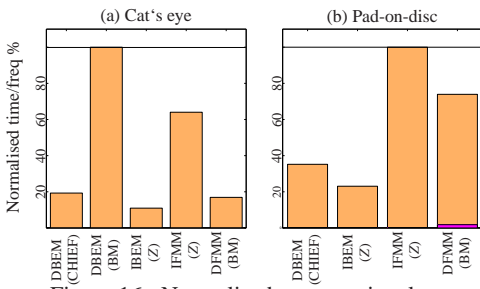


Figure 16: Normalised computational costs

**Forced Response Study** The extraction of surface velocities is essential in order to calculate the acoustic radiation by means of BEM. The differences in the forced response due to different calculation methods (modal, subspace, direct) and due to different types of excitation (point force vs uniform pressure) have been demonstrated (Figure 6). For pure mode-coupling instability in the frequency range of interest, without in-plane pad modes, subspace projection methods can be used to obtain good estimates of surface velocities, as discussed in [20]. However, the direct steady-state analysis is far more accurate as it calculates the system’s response directly in terms of its degrees of freedom and captures pure friction-induced effects (such as pad-mode instabilities [38, 39, 41]) much better. Further, a pressurised pad delivers a more realistic forced response, with a higher relative change between different loading regimes, tested for the disc alone, a pre-stressed disc and a disc in frictional contact. The computer run times, as investigated in [20], are longest for the direct steady-state analysis which is a severe disadvantage of this method, especially if larger models are investigated.

**Acoustic Study** Next, the acoustic power of the cat’s eye radiator as a global measure is analysed as it could thin out some of the methods before analysing, in detail, by means of more sensitive parameters concerned with irregular frequencies/ internal res-

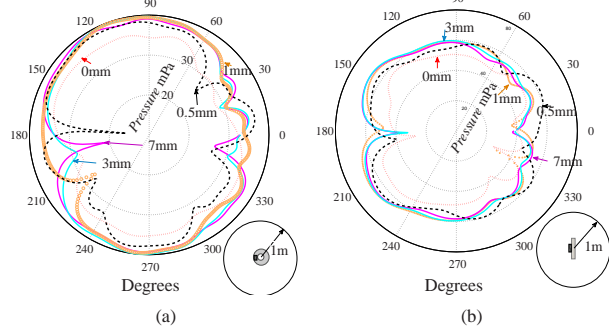


Figure 17: (color online) Directivity plots for gaps of 0.5, 1, 3 and 7mm.

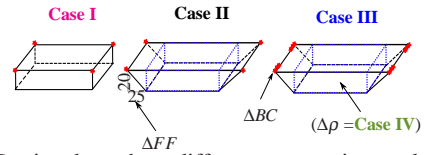


Figure 18: Depicted are three different geometries used for four different models: (Case I) baseline configuration with steel pad; (Case II) chamfers; (Case III) stiffened type boundary conditions; and (Case IV) density such that weights of pad (I) and pad (IV) equal

onances. To begin with, the analytical sphere is calculated and a plane-wave approximation is applied to the structure which show that the sphere radiates higher power than does the cat’s eye in the far-field. It is expected that the acoustic power level of the cat’s eye is slightly lower than that of a sphere as one octant is cut out which has an imposed zero velocity BC. The DBEM/BM implemented in AKUSTA, performs well and approximates the acoustic power level of a sphere. The two indirect methods of LMS both work fine, the modelling requests the correct impedance to be applied, but mostly the one of air is found to be sufficient. The IFMM, based on the formulation of the indirect method, follows the curve of the IBEM. The DBEM/ CHIEF (LMS) seems to perform fine in terms of the overall sound power level compared with the other methods. The DBEM/BM (AKUSTA) performs well as does the DFMM with Burton-Miller formulation. As mentioned earlier, acoustic power as an integral measure is not very sensitive to pressure fluctuations. Hence, the DFMM and DBEM, both working with a Burton-Miller formulation are studied in terms of their sound pressure magnitudes in the centre, and at the back, of the cat’s eye radiator. It is expected, that on the back of the cat’s eye, the sound pressure level of a sphere is approximated and it is found, that both methods perform well.

Next, the second benchmark with contacting surfaces is studied. In order to evaluate firstly the pad-on-plate then the pad-on-disc system, the acoustic power level is calculated. Here, a possible integration error due to contacting surfaces of two radiating bodies is of special interest. Hence, for the pad-on-plate system, two possibilities are evaluated: (1) the use of a wrapping mesh; and (2) no wrapping mesh.

It is found, by means of a pad-on-plate system, that the choice of wrapping mesh is not arbitrary as the *desired element length* has to be chosen such, that the seeding of the structural analysis in regions of high acoustic significance (e.g., contact patch) is matched. It can be assumed, that too coarse or too fine a mesh either under- or over-estimates the acoustic power level, respectively (see Figure 13). If no wrap is taken, an integration error does not seem to be too large except that, depending on the numerical method used, the convergence and, therefore, the computational performance, might suffer. A comparison of different methods shows that, indeed, the deviations are not too large, and that all methods tested perform sufficiently well in the prediction of radiated power. However, shortcomings are there, due mainly to integration errors or irregular frequencies which, however, are only visible under magnification. In terms of computational cost regarding only the cat’s eye radiator, preference has to be given

to the DFMM since it seems to be a sufficiently accurate method capable of calculating results very quickly due to its iterative solver. Also, the IFMM seems to have an advantage because of the incapability of the DBEM and IBEM to solve large problems at high frequencies due to large memory consumption but suffers from high computational costs, due to the large proportion of calculations in the low frequency range. Both models, definitely the cat’s eye and also the pad-on-disc were also too small for the IFMM. Due to the low frequency range involved and the relatively small size of the models, either the slower synoise solver was used more often or sub-leveling of the acoustic domain was in efficient [49]. Also, the problem of internal resonances is not overcome, which will pose a problem for a real brake system with an increased modal density. Ta-

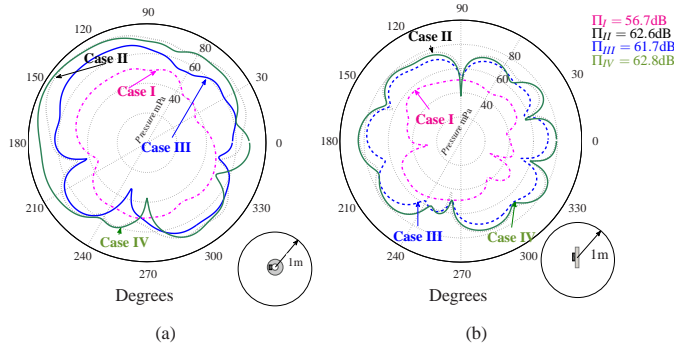


Figure 19: (colour online) Acoustic pressure (dB)g for Cases I-IV (Figure 18)

ble 2 gives an overview of the test results. Here,  $f_{irr}$ ,  $J$ , Mem, Cost stand for irregular frequencies, integration error, memory consumption and computational cost in average time/frequency, respectively. Further, the category ‘Model size (sma/med/lar)’ gives a recommendation as to whether it is feasible to calculate (small/medium/large) models by the method, respectively. Values in brackets were not evaluated here, and only estimated.

Then, by means of a gap study, the lift-off of the pad up in context with a horn effect is evaluated. No additional integration errors due to contacting surfaces are expected. The outcome of this study is, that lifting the pad up results in a horn effect which amplifies the sound pressure. As a consequence, the amplification of chamfered pads is studied. Results show that pads with chamfers produce higher sound pressure and acoustic power levels.

Table 2: Results from BEM benchmarks model  $\mathcal{A}$  and  $\mathcal{B}$

Method	$f_{irr}$ ( $\mathcal{A}$ )	$J$ ( $\mathcal{B}$ )	Mem ( $\mathcal{A}/\mathcal{B}$ )	Cost ( $\mathcal{A}/\mathcal{B}$ )	Model Size sma/med/lar
ERP	NA	NA	✓/✓	✓/✓	✓/✓(✓)
DBEM/CHIEF	✓	✓	✓/✗	✓/✓	✓/✗(✗)
DBEM/BM	✓	✗	✓/✗	✗/✗	✓/✗(✗)
IBEM	✓	✓	✗/✓	✓/✓	✓/✗(✗)
IFMM	✓	✗	✓/✓	✗/✗	✗/✗(✓)
DFFM	✓	✗	✓/✓	✓/✓	✓/✓(✓)

In conclusion it can be said, that the DFMM solver implemented in ESI/VA performed accurately (no irregular frequencies or visibly higher integration errors due to contact), was easy to apply and the fastest. Apart from that, the plane-wave approximation was a good alternative for obtaining preliminary estimates of acoustic power. Due to a lifting-off of the pad, a horn effect was evidenced and was also present for pads with chamfers which resulted in highly amplified sound pressure/power levels.

Further work should be directed towards the understanding of acoustic radiation of simplified brake systems for which complexity can be built up step by step. Also, the findings for pad-on-disc systems have to be validated for a brake system with realistic geometry, which is done at the moment. The effects of high sound power at frequencies not predicted by the CEA should be validated and studied experimentally using a pad-on-disc system. Again, this could be undertaken using a simplified brake system or a laboratory brake (e.g., as

in Giannini et al. [64]). For all analyses, especially the for realistic geometry, a high-performance workstation or a server and the use of the FAST MULTI-POLE BEM over a wide range of  $kD$  values is recommended.

ACKNOWLEDGEMENTS

This research was undertaken on the NCI National Facility in Canberra, Australia, which is supported by the Australian Commonwealth Government. The first author acknowledges receipt of a University College Postgraduate Research Scholarship (UCPRS) for the pursuit of this study and the Australian Acoustical Society for a Young Scientist’s Award to participate at the ICA2010 Conference. The authors would like to thank Eric Loesche who contributed, in the course of his Master’s thesis, some calculations using the software AKUSTA.

REFERENCES

- [1] N.M. Kinkaid, O.M. O’Reilly, and P. Papadopoulos. Automotive disc brake squeal. *Journal of Sound and Vibration*, 267:105–166, 2003.
- [2] A. Akay. Acoustics of friction. *Journal of the Acoustical Society of America*, 111(4):1525–1548, 2002.
- [3] H. Jacobsson. Aspects of disc brake judder. *Proc. Instn. Mech. Engrs. Vol. 217, Part D, Journal of Automobile Engineering*, 217:419–430, 2003.
- [4] F. Chen, F. Tan, C./Chen, C. A. Tan, and R. L. Quaglia. *Disc Brake Squeal: Mechanism, Analysis, Evaluation and Reduction/Prevention*. SAE-Society of Automotive Engineers, 2006.
- [5] H. Ouyang, W. Nack, Y. Yuan, and F. Chen. Numerical analysis of automotive disc brake squeal: a review. *Int. J. of Vehicle Noise and Vibration*, 1:207–231, 2005.
- [6] A. Papinniemi, J. Lai, J. Zhao, and L. Loader. Brake squeal: a literature review. *Applied Acoustics*, 63:391–400, 2002.
- [7] S. Oberst and J. C. S. Lai. A critical review on brake squeal and its treatment in practice. In *Internoise 2008, Shanghai*, 2008.
- [8] N. Hoffmann and L. Gaul. Friction induced vibrations of brakes: Research fields and activities. *SAE Technical Paper Series*, 2008-01-2579:1–8, 2008.
- [9] S. Marburg and B. Nolte, editors. *Computational Acoustics of Noise Propagation in Fluids - Finite and Boundary Element Methods*. Springer Verlag, 2008.
- [10] I. Harari and T. JR Hughes. A cost comparison of boundary element and finite element methods for problems of time-harmonic acoustics. *Computer Methods and Applied Mechanics in Engineering*, 97:77–102, 1991.
- [11] L. Thompson. A review of finite element methods for time-harmonic acoustics. *Journal of Acoustical Society of America*, 119(3):1315–1330, 2006.
- [12] I. Harari. A survey of finite element methods for time-harmonic acoustics. *Computational Methods in Applied Mechanical Engineering*, 195:1594–1607, 2006.
- [13] T.W. Wu. *Boundary Element Acoustics, Fundamentals and Computer Codes*. WIT - Press, 2000.
- [14] S. Marburg and S. Schneider. Performance of iterative solvers for acoustic problems. part 1: Solvers and effect of diagonal preconditioning. *Engineering Analysis with Boundary Elements*, 27:727–750, 2003.
- [15] A. Buck. *Simulation von Bremsenquietschen (Brake Squeal)*. PhD thesis, Lehrstuhl für Baumechanik, Technische Universität München, 2008.
- [16] M. Lee and R. Singh. Analytical formulations for annular disk sound radiation using structural modes. *Journal of Acoustical Society of America*, 95(6):3311–3323, June 1994.
- [17] H. Lee. *Modal Acoustic Radiation Characteristics of a Thick Annular Disk*. PhD thesis, Graduate School of The Ohio State University, 2003.
- [18] H. Lee and R. Singh. Determination of sound radiation from a simplified disc-brake rotor by a semi-analytical method. *Noise Control Engineering Journal*, 52(5):225–239, Sept-Oct 2004.

- [19] H. Lee and R. Singh. Acoustic radiation from out-of-plane modes of an annular disk using thin and thick plate theories. *Journal of Sound and Vibration*, 282(1-2):313–339, April 2005.
- [20] S. Oberst and J.C.S. Lai. Numerical prediction of brake squeal propensity using acoustic power calculation. In *Proceedings of ACOUSTICS 2009*, 2009.
- [21] R.A. AbuBaker and H. Ouyang. A prediction methodology of disk brake squeal using complex eigenvalue analysis. *Int. J. Vehicle Design*, 46:416–435, 2008.
- [22] S. Marburg and S. Amini. Cat’s eye radiation with boundary elements: comparative study on treatment of irregular frequencies. *Journal of Computational Acoustics*, 13:21–45, 2005.
- [23] K. A. Cunefare, G.G. Koopmann, and K. Brod. A boundary element method for acoustic radiation valid for all wavenumbers. *Journal of the Acoustical Society of America*, 85:39–48, 1989.
- [24] T.W. Wu and A.F. Seybert. An efficient boundary element algorithm for multi-frequency acoustical analysis. *Journal of the Acoustical Society of America*, 94:447–452, 1993.
- [25] E. Loesche. Energiegrößen basierte Beitragsanalyse beim akustischen Außenraumproblem. Master’s thesis, Fakultät Maschinenwesen, Institut für Festkörpermechanik, 2009.
- [26] *VA One 2009 (ESI), Vibro-Acoustics, User’s Guide*.
- [27] E. Perrey-Debain, J. Trevelyan, and P. Bettess. Plane wave interpolation in direct collocation boundary element method for radiation and wave scattering: numerical aspects and applications. *Journal of Sound and Vibration*, 261(5):839–858, 2003.
- [28] S. Marburg. Six elements per wavelength, is this enough? *Journal of Computational Acoustics*, 10(1):25–51, March 2002.
- [29] S. Oberst, J. C. S. Lai, S. Moore, A. Papinniemi, S. Hamdi, and D. Stanef. Chaos on brake squeal. In *Internoise 2008, Shanghai*, 2008.
- [30] A. Cote, N. Atalla, and J.-L. Guyader. Vibroacoustic analysis of an un baffled rotating disk. *Journal of the Acoustical Society of America*, 103(3):1483–1492, 1998.
- [31] Dassault Systemes. *ABAQUS/CAE User’s MANUAL*, 2007.
- [32] Dassault Systemes. *ABAQUS Technology Brief: Automotive Brake squeal Analysis Using a Complex Modes Approach*, 2007. TB-05-BRAKE-1.
- [33] J. Awrejcewicz and P. Olejnik. Analysis of dynamic systems with various friction laws. *Applied Mechanics Reviews*, 58:389–411, November 2005.
- [34] M. Müller and G.P. Ostermeyer. A cellular automaton model to describe the three-dimensional friction and wear mechanism of brake systems. *Wear*, 263:1175–1188, 2007.
- [35] S.C. Brenner and S. Ridgway. *The Mathematical Theory of Finite Element Methods*. Berlin, New York: Springer-Verlag, 2008.
- [36] R. Barlow. Some new surfaces with  $p_g = 0$ . *Duke Mathematical Journal*, 51(4):889–904, 1984.
- [37] Dassault Systemes. *ABAQUS 6.9-EF, Benchmark manual*.
- [38] S. Oberst and J.C.S. Lai. Numerical study of friction-induced pad mode instability in disc brake squeal. In *20th International Congress on Acoustics (ICA 2010) in Sydney, 23 - 27 August, Australia*, 2010.
- [39] S. Oberst and J.C.S. Lai. Acoustic radiation due to friction-induced pad mode instability in disc brake squeal. In *20th International Congress on Acoustics (ICA 2010) in Sydney, 23 - 27 August, Australia*, 2010.
- [40] D. Guan and J. Huang. The method of feed-in energy on disc brake squeal. *Journal of Sound and Vibration*, 261:297–307, 1994.
- [41] S. Oberst and J.C.S. Lai. Uncertainty modelling in detecting friction-induced pad mode instabilities in disc brake squeal. In *20th International Congress on Acoustics (ICA 2010) in Sydney, 23 - 27 August, Australia*, 2010.
- [42] Dassault Systemes. *ABAQUS 6.7-1, Theory Manual*.
- [43] N. Hinrichs, M. Oestreich, and K. Popp. On the modelling of friction oscillators. *Journal of Sound and Vibration*, 216(3):435–459, 1998.
- [44] F. Chen. Automotive disk brake squeal: an overview. *Int. J. Vehicle Design*, 51(1/2):39–72, 2009.
- [45] S. Oberst and J. C. S. Lai. Numerical analysis of a simplified brake system. In *NOVEM2009, Keble College, Oxford, England, 5-8 April*, 2009.
- [46] J. Dai. *Surface Mobility of a Thin Plate over a Rectangular Contact Area*. PhD thesis, School of Aerospace and Mechanical Engineering, University College, The University of New South Wales, 1999.
- [47] N. Coudeyras, J.-J. Sinou, and Nacivet. A new treatment of predicting the self-excited vibrations of nonlinear systems with frictional interfaces: The constrained harmonic balance method, with application to disc brake squeal. *Journal of Sound and Vibration*, 319:1175–1199, 2009.
- [48] H. Gao, C. Ye, and G. Cheng. Deformation behaviours and critical parameters in microscale laser dynamic forming. *ASME Journal of Manufacturing Science and Engineering*, 131:1–11, 2009.
- [49] *LMS Virtual Lab R8A, help manual*.
- [50] J.C.F. Telles. A self-adaptive co-ordinate transformation for efficient numerical evaluation of general boundary element integrals. *International Journal for Numerical Methods in Engineering*, 24:959–973, 1987.
- [51] F. Fahy and P. Gardonio. *Sound and Structural Vibration: Radiation, Transmission and Response*. Academic Press, Sydney, 2007.
- [52] R.D. Ciskowski C.A. Brebbia. *BEM in Acoustics*. Kluwer Academic Publishers, 1989.
- [53] E. Hairer, S. Nørsett, and G. Wanner. *Solving ordinary differential equations I: Nonstiff problems*. Springer Verlag, Berlin., 2 edition, 1993.
- [54] J. Wang and T.-K. Tsay. Analytical evaluation and application of the singularities in boundary element method. *Engineering Analysis with Boundary Elements*, 29:241–256, 2005.
- [55] S. Amini. On the choice of the coupling parameter in boundary integral formulations of the exterior acoustics problem. *Applicable Analysis*, 35:75–92, 1989.
- [56] T.J. Rudolph, F.J. Rizzo, M. Guiggiani, and G. Krishnasamy. A general algorithm for the numerical solution of hypersingular boundary integral equations. *Journal of Applied Mechanics*, 59:604–614, 1992.
- [57] R. Silva, editor. *Acoustic and elastic wave scattering using boundary elements*, volume 18. Southampton: Computational Mechanics Publications, 1993.
- [58] M. Fischer. *The Fast Multipole Boundary Element Method and its Application to Structure-Acoustic Field Interaction*. PhD thesis, Fakultät Maschinenbau der Universität Stuttgart, Institut A für Mechanik, 2004.
- [59] LMS. *Valid frequency range for the FMBEM-solver*, 2008. from website.
- [60] S. Chaillat, M. Bonnet, and J.-F. Semblat. A fast multipole method formulation for 3d elastodynamics in the frequency domain. *Comptes Rendus Mecanique*, 335:714–719, 2007.
- [61] N.A. Gumerov and R. Draiswami. A broadband fast multipole accelerated boundary element method for the three dimensional helmholtz equation. *Journal of the Acoustical Society of America*, 125(1):191–205, January 2009.
- [62] A.J. Burton and G.F. Miller. The application of integral equation methods to the numerical solution of some exterior boundary-value problems. *Proceedings of the Royal Society of London*, 323:201–220, 1971.
- [63] R.A. Graf, C.-Y. Kuo, P. Dowling, and W.R. Graham. On the effect of a tyre/road interface, part i: Experiment and computation. *Journal of Sound and Vibration*, 256(3):417–431, 2002.
- [64] O. Giannini and A. Sestrieri. Predictive model of squeal noise occurring on a laboratory brake. *Journal of Sound and Vibration*, 296:583 – 601, 2006.